A mathematical model for diffusion with induced crystallization: 1.

Christopher J. Durning* and William B. Russel
Textile Research Institute, and Department of Chemical Engineering, Princeton University, Princeton, New Jersey 08544, USA
(Received 31 October 1983; revised 16 February 1984)

During the sorption of swelling agents in amorphous, but crystallizable, glassy polymers local crystallization takes place. Previous work has shown that the weight gain and overall crystallization kinetics depend on the polymer/penetrant interactions and the dimensions of the sample. In this paper we propose a mathematical model for the process which includes four important effects: time dependent polymer swelling, blocking of diffusion by crystallites, occlusion of penetrant by developing crystallites, and macrovoid formation. The model predicts four limiting regimes of behaviour according to the values of the dimensionless crystallization rate, Ω, and the dimensionless sample half thickness, λ_p. Analytical solutions are developed for each limiting case, with the corresponding criteria for their application to real systems. The model successfully predicts the variety of behaviours observed experimentally.

(Keywords: macrovoids; cavitation; solvent induced crystallization; anomalous diffusion; non-Fickian diffusion)

INTRODUCTION

Certain crystallizable polymers can be obtained in the glassy state without significant levels of crystallinity. This occurs when macromolecules with relatively stiff backbones are rapidly quenched from the amorphous melt. The time necessary for such molecules to crystallize greatly exceeds that required to quench the melt to the glassy state. The result is an amorphous, crystallizable glass, hindered kinetically from assuming its energetically favoured (semi-crystalline) configuration. Introduction of an interactive diluent removes these hindrances by plasticizing the material locally; hence, the glass will crystallize during the permeation of the diluent into the specimen. Previous work[1,2] focused on the nature of the interaction between a polymer diluent pair. Interactive liquids are generally condensable, low molecular weight, organic compounds soluble enough in the polymer to depress the glass transition temperature below the environmental temperature. This implies the existence of a threshold concentration necessary to induce crystallization. In the following sections we consider situations where the external penetrant activity significantly exceeds the threshold level. Diffusion in crystallizable glasses below the threshold would resemble the sorption of vapours in amorphous, glassy polymers. Appropriate descriptions of this situation were reviewed by Frisch[3] as diffusion and sorption below the glass transition.

Diffusion with induced crystallization has been studied for a variety of polymers, all with relatively stiff backbones. These include cellulosics[4], poly(ethylene terephthalate) (PET)[5-12], bisphenol-A-polycarbonate (PC)[13-20], poly(ethylene 2,6-naphthalate) (PEN)[21], isotactic polystyrene (IPS)[22], poly phenyleneoxide (PPO)[23], and polysulphone[24]. The process can be discussed in terms of three coupled phenomena: the transport of the diluent into the polymer, the local crystallization of the specimen, and the formation of macrovoids (i.e. 'cavitation') which results from the first two. The present work proposes a mathematical model for this coupled transport and morphological development. Before proceeding, we review briefly the significant aspects of this problem.

BACKGROUND

Moving boundary phenomena

In PET[8,9], PC[16,17,20] and IPS[22], the migration of interactive diluents is accompanied by a moving boundary reminiscent of those observed during non-Fickian diffusion in noncrystallizable glassy polymers[25]. The boundary separates a region of highly swollen material, capable of crystallization, from a relatively unperturbed glass. While much of the recent literature[8,9,11,12] claims this diffusion is Fickian, the moving boundary suggests it is essentially non-Fickian. Kambour[14] recognized this fact for polycarbonate systems. In PET films exposed to highly interactive diluents, Makarewicz and Wilkes[9] observed a crack spanned by plastically deformed material preceding the advancing boundary. The crack did not appear for less interactive liquids. Turska[16,17] noted 'pinlike crazes' perpendicular to the boundary in PC films immersed in a variety of ketones. Current theories for non-crystallizable glassy polymers relate the moving boundary's velocity to the mechanical response of the polymer under osmotic swelling stresses. The response is system specific; microfailure or crazing mechanisms apply for severe interactions[26] while a phlegmatic viscous response[27,28] appears appropriate for other systems. Crystallizable systems of practical importance evidently involve the former.

Desai[8] and Makarewicz[9] measured the kinetics of

* Current address: Department of Chemical Engineering and Applied Chemistry, Columbia University, New York, 10027.

0032-3861/85/010119-12S03.00
© 1985 Butterworth & Co. (Publishers) Ltd.

moving boundary penetration in thick PET slabs for a variety of diluents. The penetration depth generally increased linearly with $\sqrt{t}$, indicating a diffusional limitation. Turska[16,17] and Wilkes[20] found similar behaviour for ketones in PC.

Weight gain kinetics

The weight gains in the systems discussed above also generally increase linearly with $\sqrt{t}$, but some systematic deviations from this are known. In thick PET films[9], weight gain continues even after complete penetration of the sample by the moving boundary. In thin PC[14,15,19] and IPS[22] films weight gain initially increases linearly with time (i.e. Case II behaviour). Weight gain sometimes increases more slowly than $\sqrt{t}$ and uptake curves with peaked maxima have also been reported for PET[7,9], PC[13-15,17,19,20], and IPS[22] systems. A systematic presentation of weight gain anomalies is given in a companion publication[29].

Crystalline morphology

Desai[8] and Makarewicz[10] determined the nucleation behaviour and crystalline morphology of PET crystallized by liquids using small angle light scattering (SALS) and scanning electron microscopy (SEM). SALS revealed spherulitic crystallites which developed immediately behind the moving boundary from rod-like precursors. SEM showed uniformly sized spherulites suggesting athermal nucleation. Spherulite sizes (2–3 μm) were not strongly solvent or temperature dependent. Parlapiano and Wilkes[20] found similar morphologies in PC systems.

Crystallization kinetics

During solvent sorption, penetrant molecules migrate towards the film's centreline, plasticizing the internal portions of the sample. Crystallites then develop and grow to their maximum size. Clearly, two rate processes govern the overall crystallization rate: solvent migration into the sample's interior and crystallite growth in the plasticized elements of the sample. The slower process will control the overall crystallization rate, hence, the experimentally measured crystallization kinetics are discussed in terms of a rate limiting process.

Sheldon[5,6] measured the overall crystallization kinetics by density for PET films (0.02–0.04 cm thick) immersed in ketones; the data indicated a diffusion controlled process. Desai[8] performed transient wide angle X-ray scattering experiments and also found diffusion controlled crystallization in PET films (11.5 mm thick) exposed to dioxane and nitromethane.

Crystallization in PC systems apparently departs from diffusion control. For example, light microscopy[16,17] showed a distinct crystallization 'front' lagging the moving boundary for PC films immersed in ketones, indicating that crystallites develop slowly following plasticization. Cohen *et al.*[19] observed sorption overshoots in thin PC films exposed to acetone (but not in thicker specimens) which were attributed to crystallite growth control of the overall crystallization kinetics; solvent migrates into the film in a relatively short time and subsequent crystallite growth occludes solvent causing desorption to produce an overshoot[7,10,14,15,17,22].

Zachmann[7] developed a mathematical model for the overall crystallization kinetics during solvent sorption in films. The simplifying assumptions were:

(a) solvent diffuses into the film as a discontinuous front advancing linearly with $\sqrt{t}$,

(b) spherulitic crystallites develop behind the front from pre-existing nucleii (athermal nucleation), and

(c) an Avrami equation governs the volume fraction crystallized at a given location as a function of time *after* the front arrives.

Zachmann's treatment predicts overall crystallization kinetics controlled either by solvent diffusion or crystallite growth depending on the ratio of the time scale for film penetration by the front to that for complete crystallite development.

Makarewicz[10] theoretically analysed the effect of interactive solvents on the crystallite growth rate in PET by adapting the kinetic nucleation model for crystallization developed by Hoffman and Lauritzen[30]. He found that the additional free volume contributed to the system by the solvent enhanced the growth rate by 1–2 orders of magnitude. Using experimentally measured solvent penetration rates, Makarewicz estimated the time scale ratio in Zachmann's model for several PET/solvent systems and predicted correctly solvent diffusion control of the overall crystallization kinetics in PET films thicker than 0.1 mm.

Macrovoid formation

Macrovoids refer to the large pores resulting from crystallization in the swelled state. Previous publications[2,10-12,20,21] refer to macrovoid formation as cavitation. Qualitative discussions of surface cavitation in connection with fibre systems[2] have attributed it to solvent rejection from crystallites developing in saturated surface layers. However, no clear understanding of the circumstances required for the formation of macrovoids exists.

Makarewicz[9] and Desai[8] have done the most complete experimental investigations of macrovoid formation. In their thick PET specimens, macrovoids developed in surface layers almost immediately upon contact with interactive liquids. Contact with less interactive liquids, or with saturated vapours, produced only minor surface roughening. Wilkes[20,21] recorded similar characteristics for PEN and PC surfaces. In the PET studies, the thick specimens showed no internal macrovoids.

Under certain conditions, internal macrovoids are inferred or observed directly. In extremely thin PET films crystallized by interactive liquids, Lawton and Cates[31] measured abnormally low densities and suggested that macrovoids occurred throughout the thin film. Titow *et al.*[15] also found reduced densities in solvent crystallized PC films. Using small angle X-ray scattering (SAXS), Jameel[12] inferred small internal voids in thin, slightly oriented PET films crystallized in *N,N* dimethylformamide. Electron microscopy detected internal macrovoids directly in PC crystallized by acetone[20] and in PEN crystallized by aniline and dioxane[21].

MODEL DEVELOPMENT

Previous efforts in modelling diffusion with induced crystallization focused on individual aspects of the overall phenomenon, such as the transport rates[19] or the overall crystallization kinetics[7,10]. The model developed below combines the transport, crystallization and macrovoid

Table 1 Estimate of threshold concentration and ratio of threshold to solubility for isotactic polystyrene at 25°C

	Liquid	c^* [g cm^{-3}]	c^*/c_0
a	Acetone	0.09	0.02
b	Methylene chloride	0.15	0.07

Calculations use equations (1) and (2) from ref. (2)
Physical data from ref. (19) and (35)
a x^0 for acetone at 30°C
b x^0 for methylene chloride at 85% activity

phenomena to provide an understanding of their coupling.

Assumptions

Four simplifications allow a compact mathematical representation of diffusion with simultaneous crystallization:

(a) *Microscopic gradients do not significantly affect the overall crystallization kinetics.* Developing crystallites tend to occlude mobile penetrants thereby elevating the penetrant concentration at the crystallite surface above that in the adjacent amorphous polymer as, for example, during the redistribution of additives in crystallizing polypropylene[32]. This effect must be accounted for when the penetrant level strongly influences the crystallite growth rate. However, if the penetrant's diffusion velocity greatly exceeds the radial velocity of the growing spherulites, i.e.

$$\frac{\text{radial velocity of spherulite}}{\text{microscopic diffusion velocity}} = \frac{G}{D/l} = \frac{lG}{D} \ll 1$$

then no significant elevation of the penetrant concentration occurs and the average concentration in the adjacent amorphous polymer governs the crystallite growth rate. Such is clearly the case for PET-diluent systems[10] for which $G \cong 50\,\text{nm s}^{-1}$, l (the length scale of the amorphous regions) $\cong 2000$ nm, and D (the penetrant diffusivity) $\cong 10^7\,\text{nm}^2\,\text{s}^{-1}$, so that $lG/D \cong 10^{-2}$.

(b) *Penetrant dissolution and transport occurs only in amorphous regions.* A two phase model of semicrystalline polymers (impermeable crystallites embedded in an amorphous matrix) adequately explains the effect of crystallinity on the transport of small molecules[33]. We adopt this model during the development of crystallinity, thereby ignoring interphase material with properties intermediate between amorphous and crystalline regions.

(c) *Immobilization of the diluent is negligible.* Some diluent is unavoidably trapped in developing crystallites, but the amounts typically detected are quite small (≈ 4 wt% for methylene chloride in PET[34]).

(d) *Local expansion during swelling occurs instantaneously, except near the moving boundary.* Here we assume that the time dependent physical processes responsible for the transformation of the glassy polymer to a swollen rubber are confined to the immediate vicinity of the moving boundary. Sarti *et al.*[26,35] employed this assumption in their thermodynamic treatment of solvent crazing in atactic polystyrene. This requires that the penetrated portion of the polymer be severely plasticized, such that the material's response time is short. The assumption is valid when the external penetrant concentration greatly exceeds the threshold for chain mobility characteristic of the rubbery state or, equivalently, if the threshold concentration lies well below the ultimate solubility of the diluent in the polymer, c_0. In such cases the amount of penetrant contained in the glassy region ahead of the boundary is very small. Typical interactive diluents in PET satisfy this condition[2], as do the IPS systems noted in *Table 1*. The assumption is less satisfactory for PC systems[2]. When the external activity only slightly exceeds the threshold one must account for solvent in the glassy region and for the time dependent internal processes throughout the specimen, as in Thomas and Windle's[28] treatment of diffusion.

Figure 1 shows a schematic concentration profile consistent with the above assumptions. (The symbols used in *Figure 1* are described later in this paper.)

Equations of change

On the basis of assumption (d), one can ignore the transport of solvent ahead of the moving boundary. An appropriate one dimensional description for the transport behind the boundary in laboratory fixed Cartesian coordinates is

$$\frac{\partial}{\partial x} D_E(f,c) \frac{\partial c}{\partial x} - \frac{\partial}{\partial x}(1-f)uc = \frac{\partial}{\partial t}(1-f)c \qquad (1a)$$

$$\frac{\partial \rho}{\partial t} + \frac{\partial}{\partial x} u\rho = 0 \qquad (1b)$$

$$\frac{\partial f}{\partial t} = g(c,f) \qquad (1c)$$

$$\rho = \rho(c,f) \qquad (1d)$$

with c the diluent concentration in the amorphous regions, f the volume fraction crystallized and ρ the overall polymer density. The equation (1a) describes diluent transport due to molecular diffusion and bulk flow. A diffusion coefficient, D_E, referred to the polymer-fixed frame[36] characterizes the former. D_E depends on

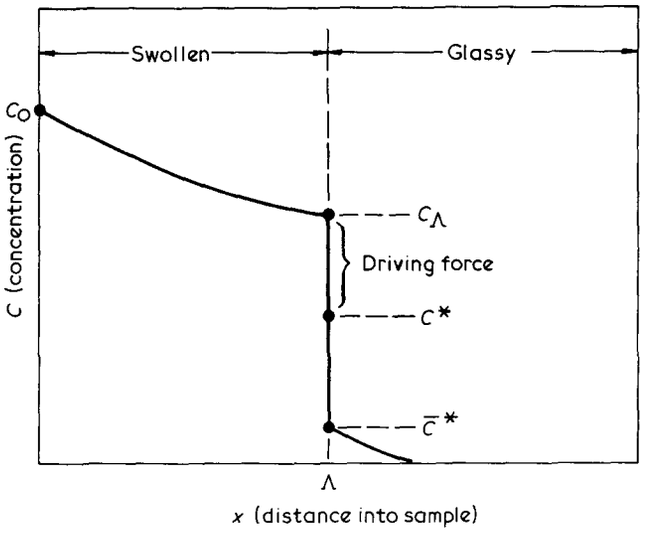

Figure 1 Schematic concentration profile during diffusion with induced crystallization

concentration and crystallinity. Swelling (i.e. distension of the sample) causes bulk flow with a mass average velocity u.

Equation (1b) is a polymer mass balance. The polymer mass density, ρ, represents a local average over a volume larger than a crystallite but smaller than the length scale for changes in diluent concentration.

Equation (1c), describing the local change in the crystalline volume fraction, contains a constitutive relationship, $g(c,f)$, accounting for the influence of concentration and crystallinity on the local rate of crystallization.

Equation (1d), an 'equation of state' for the swollen, crystallizing polymer, expresses the polymer density in terms of concentration and crystallinity. Equations (1a)–(1d), together with appropriate initial and boundary conditions, determine the transient profiles for c, ρ, u and f during diffusion with induced crystallization.

Initial and boundary conditions

Assuming instantaneous surface saturation, appropriate initial and boundary conditions for sorption in an initially dry film are

$$c(x,0)=0 \quad \text{for } 0<x<\Lambda$$

$$c(0,t)=c_0 \quad \text{for } t>0$$

$$-D_E\frac{\partial c}{\partial x}+[(1-f)uc]=[(1-f)c]\frac{d\Lambda}{dt} \quad \text{for } x=\Lambda$$

where Λ is the position of the moving boundary. The last relationship, the moving boundary condition, expresses conservation of solvent at the rubber/glass interface neglecting the solvent in the glass.

In the glassy region near the moving boundary, polymer molecules respond to swelling forces at a finite rate. We account for this kinetic process through a semi-empirical relationship adopted from Astarita[37,38]

$$\frac{d\Lambda}{dt}=K[c(\Lambda)-c^*]^n$$

$$\Lambda(0)=0$$

where c^* is the threshold concentration on the rubber side of the interface (*Figure 1*). This equation relates the rate of swelling by n^{th} order kinetics to the excess solvent concentration above the threshold on the rubber side. Curve fitting of swelling data in noncrystallizable glassy polymers indicates $n\cong 2$–3.

Sarti[26,35] has shown this approach to be relevant when crazing occurs at the moving boundary. Here, the penetrant activity at the front depresses the chemical potential of the polymer on the swollen side below that in the adjacent glass, resulting in an osmotic tension in the glass which drives the crazing process. Considering the visual evidence for cracking or crazing at the boundary in glassy PET and PC, this approach seems more appropriate than that postulated by Thomas and Windle[27,28] where the osmotic tension causes viscous flow near the boundary.

The effective diffusivity, D_E

According to Peterlin[33], $D_E=\Psi D_a/B$, where Ψ is the geometric impedance factor, B is the blocking factor, and D_a is the amorphous phase diffusivity. $\Psi(<1)$ accounts for the increase in diffusion path length with crystallinity since penetrant molecules must migrate around crystallites. It depends on the degree of crystallinity and the specific crystalline morphology. We assume Ψ equals the amorphous fraction by analogy with the diffusion of oxygen, nitrogen, carbon dioxide, methane[39] and water[41] in thermally crystallized, unoriented PET. The blocking factor, $B(>1)$, accounts for the portion of amorphous polymer ineffective for transport, such as 'dead end' passages, or extremely narrow channels between crystalline lamellae. It can be absorbed into an effective amorphous diffusivity, D, leaving $D_E=D(1-f)$.

The effect of concentration on the diffusivity can be accommodated rather neatly. For organic solvents, the free volume theory[42] predicts a precipitous rise in diffusivity at low concentrations, culminating in a maximum for the highly swollen material. We approximate this behaviour by a discontinuous diffusivity, D_a, which jumps from a negligible value below some critical concentration to a finite value above the critical level. Choosing the critical concentration as the threshold value implies a constant diffusivity in the rubbery polymer behind the front and a negligible amount of solvent in the glass ahead of the front, consistent with assumption (d).

Local crystallization rate

Following Stein and Mirsa[43] the growth rate of a single isolated spherulite of radius r is

$$\frac{dV_c}{dt}=4\pi r^2\frac{dr}{dt}=4\pi r^2 G(c)$$

where V_c is the spherulite's volume. The radial growth rate, $G(c)$, depends only on the external diluent concentration. The total growth rate for N_s spherulites in a volume V_E, assuming simultaneous (i.e. athermal) nucleation, is

$$\frac{dV_T}{dt}=4\pi f^2 G(c)N_s\left(\frac{V_T^\infty-V_T}{V_T^\infty}\right)$$

The correction factor in parentheses accounts for spherulite impingement, which limits the total volume of the spherulites, V_T, to V_T^∞. Since

$$\frac{N_s 4}{V_E 3}\pi r^3=\frac{V_T}{V_E}=f$$

then

$$\frac{df}{dt}+f\frac{d\ln V_E}{dt}=\left(36\pi\frac{N_s}{V_E}\right)^{1/3}\frac{G(c)}{f_0}f^{2/3}(f_0-f)$$

with $f_0=V_T^0/V_E$. Neglecting changes in V_E during crystallization, the right hand side of the last equation becomes the function $g(c,f)$ in (1). We require an initial condition, $f=f_1\ll 1$, interpreted as the volume fraction of nuclei frozen into the glass ahead of the moving boundary. These may be incipient nuclei retained from the melt, glassy heterogeneities, or nucleating agents.

Influence of bulk transport

Scaling the transport equations with a time scale (t^*) and length scale (x^*) for which diffusion and swelling have

Table 2 Solvent volume fraction in amorphous polymer and polymer density at saturation

	Liquid	v_1^0	ρ_0 (g cm^{-3})	$\Delta\rho_0/\rho^*$
PET[a]	Acetone	0.36	1.2	0.10
	Nitromethane	0.38	1.1	0.15
	Dioxane[c]	0.47	1.0	0.22
	Methylene chloride	0.54	1.0	0.27
	Dimethyl formamide	0.56	0.8	0.43
PC[a]	Acetone	0.40	0.9	0.24
	Carbon tetrachloride	0.51	0.8	0.32
IPS[b]	Acetone	0.26	0.9	0.17
	Methylene chloride	0.37	0.8	0.27

[a] Physical data from ref. 2
[b] Physical data from ref. 22
[c] Physical data from ref. 9 and CRC Handbook, 46th edition; value of f_0 from unpublished results

comparable rates reveals the relative importance of bulk transport through the magnitude of the resulting dimensionless constants in the convection terms. Equating the characteristic distances penetrated by diffusion through swollen polymer and by the moving boundary, i.e.

$$x^* = \sqrt{Dt^*} = U_0 t^*$$

gives $t^* = D/U_0^2$ and $x^* = D/U_0$. Here U_0 represents the characteristic velocity of the moving boundary. Suitable dimensionless variables then follow as[37,38]

$$\tau = t/t^* = tU_0^2/D$$
$$\xi = x/x^* = xU_0/D$$
$$\lambda = \Lambda/x^* = \Lambda U_0/D$$

Convenient choices for the dimensionless penetrant concentration and polymer density are $\gamma = (c - c^*)/(c_0 - c^*)$ and $\Gamma = (\rho - \rho^*)/(\rho_0 - \rho^*) = \Delta\rho/\Delta\rho_0$, respectively, where ρ^* is the polymer density at the moving boundary and $\Delta\rho_0$ is the ultimate change in ρ.

Introducing the dimensionless variables into equation (1) gives the scaled transport equations

$$\frac{\partial}{\partial\xi}(1-f)\frac{\partial\gamma}{\partial\xi} - (\Delta\rho_0/\rho^*)\frac{\partial}{\partial\xi}(1-f)v(\gamma+q) = \frac{\partial(1-f)(\gamma+q)}{\partial\tau} \tag{2a}$$

$$\frac{\partial\Gamma}{\partial\tau} + \frac{\Delta\rho_0}{\rho^*}\frac{\partial}{\partial\xi}(v\Gamma) + \frac{\partial v}{\partial\xi} = 0 \tag{2b}$$

with $v = u\rho^*/U_0\Delta\rho_0$ and $q = c^*/(c_0 - c^*)$ representing the dimensionless mass average velocity and threshold concentration, respectively.

For small $\Delta\rho_0/\rho^*$ equations (2a) and (2b) decouple, and the convection term in the penetrant transport equation can be neglected. We adopt this approximation for mathematical simplicity thereby neglecting volumetric changes accompanying mixing and crystallization as done in the derivation of $g(c,f)$.

To support this approximation, we have estimated $\Delta\rho_0/\rho^*$ for a variety of systems using additive mixing rules for amorphous polymer and solvent and for amorphous and crystalline phases. Then, the volume fraction diluent at saturation, v_1^0, and the corresponding overall polymer density, ρ_0, are

$$v_1^0 = x^0\left[\frac{f_0}{(1-f_0)}\rho_c + \rho_a\right](\rho_s + x^0\rho_a)$$

$$\rho_0 = f_0\rho_c + (1-f_0)(1-v_1^0)\rho_a$$

where x^0 is the ultimate overall mass fraction of solvent, f_0 the ultimate crystallinity, and ρ_a and ρ_c the amorphous and crystalline polymer densities, respectively. Taking ρ^* as the amorphous polymer density gives the values listed in *Table 2* for $\Delta\rho_0/\rho^*$. The ratio is acceptably small in the first few PET systems and the first IPS system, but unfortunately is appreciable in the remainder.

MATHEMATICAL MODEL

The approximation of small $\Delta\rho_0/\rho^*$ leads to the following dimensionless expressions for the coupled transport and morphological development during sorption in initially dry films:

$$\frac{\partial}{\partial\xi}(1-f)\frac{\partial\gamma}{\partial\xi} = \frac{\partial(1-f)(\gamma+q)}{\partial\tau} \tag{3a}$$

$$\gamma(0,0) = 1 \tag{3b}$$

$$\gamma(\xi,0) = 0 \text{ for } 0 < \xi < \lambda \tag{3c}$$
$$\gamma(0,\tau) = 1$$

$$-\left.\frac{\partial\gamma}{\partial\xi}\right|_\lambda = (\gamma+q)_\lambda\frac{d\lambda}{d\tau} \tag{3d}$$

$$\frac{d\lambda}{d\tau} = \gamma^n\Big|_\lambda;\ \lambda(0) = 0$$

$$\frac{\partial f}{\partial\tau} = \Omega h(\gamma) f^{2/3}(f_0 - f) \tag{3e}$$

$$f(0) = f_1$$

Although written for semi-infinite media, the above readily adapt to films with a dimensionless sample half depth λ_p by replacing the moving boundary condition with a no flux condition when $\lambda = \lambda_p$. The dimensionless crystallization rate

$$\Omega = \frac{D}{U_0^2}\left(36\pi\frac{N_s}{V_E}\right)^{1/3}\frac{G_0}{f_0}S$$

represents the ratio of the characteristic time for transport, t^*, to that for complete spherulite development. Here, G_0 is the pre-exponential factor in the expression for the spherulite's radial growth rate[10,29,30], $G(\gamma)$, while $S=G_{max}/G_0=\max(0<\gamma<1)\{G(\gamma)/G_0\}$ is the maximum value of $G(\gamma)/G_0$ in the concentration interval experienced by the amorphous, rubbery polymer. The O(1) function $h(\gamma)=G(\gamma)/G_0S$ accounts for the concentration dependence of the spherulite's radial growth rate. Both S and $h(\gamma)$ are affected by the nature of the solvent and temperature. Details of their evaluation are given elsewhere[29,34].

Macrovoid formation

Examination of equation (3a–e) reveals a coupling which provides the basis for describing macrovoid formation. Since the amorphous fraction appears in the accumulation term of the diffusion equation, crystallization produces an apparent source of solvent due to the expulsion of diluent from developing crystallites. Hence, crystallization tends to elevate local concentrations above the boundary values, ultimately leading to local saturation and phase separation. This coupling produces additional moving boundaries delimiting the regions of saturation and phase separation within the material. The solution of equation (3a–e) determines the position of such boundaries, $\lambda_s(\tau)$, which separate saturated regions from areas where gradients still exist. We will discuss this embedded moving boundary problem by considering a single saturation boundary moving monotonically away from the sample surface. In this case the domain of the diffusion equation in equation (3a–e) becomes $\lambda_s(\tau)<\xi<\lambda(\tau)$ with $\gamma(\lambda_s(\tau),\tau)=1$ as the lefthand boundary condition. Within the region $0<\xi<\lambda_s(\tau)$, the condition $\gamma=1$ replaces the diffusion equation, while the crystallization equation still applies throughout the penetrated portion.

Within saturated regions, the extent of phase separation can be related to the local crystallization. Neglecting possible solvent transport via pressure driven flow, the solvent is conserved everywhere within the saturated domain, therefore

$$(1-f-\varepsilon)c_0+\varepsilon\rho_s=\text{constant}$$

where ε is the local void fraction. Substituting v_1^0 for c_0/ρ_s and noting that $\varepsilon=0$ when saturation first occurs leads to

$$\varepsilon(\xi,\tau)=\frac{v_1^0}{(1-v_1^0)}[f(\xi,\tau)-f^c(\xi)] \text{ for } 0\leqslant\xi\leqslant\lambda_s(\tau) \qquad (4)$$

where $f^c(\xi)$ is the crystallinity when phase separation commences, that is, when the saturation boundary first reaches ξ. Equation (4) shows that the maximum possible voidage occurs when $f^c=f_1\cong 0$, i.e. when the polymer saturates prior to any appreciable crystallization.

The single saturation boundary discussed above provides a convenient framework for developing equation (4) but does not necessarily represent the actual circumstances. For example, saturation boundaries do not appear in semi-infinite media since diffusional gradients always transport solvent away from regions of rapid accumulation[29]. Conversely, in finite slabs, two saturation boundaries may appear[34].

Integrated properties

The most important predictions are the solvent uptake and the overall volume fraction crystallized. The total weight gain equals the integral of the solvent concentration over the penetrated region

$$\omega_T(\tau)=\int_0^{\lambda}\{\varepsilon(\xi,\tau)\rho_s^*+[1-f(\xi,\tau)-\varepsilon(\xi,\tau)][\gamma(\xi,\tau)+q]\}d\xi$$
$$=\int_0^{\lambda_s}[\varepsilon\rho_s^*+(1-f-\varepsilon)(1+q)]d\xi+\int_{\lambda_s}^{\lambda}(1-f)(\gamma+q)d\xi \qquad (5)$$

The second expression resolves the penetrated portion into saturated and unsaturated regions. For finite media, the relative weight gain follows from normalization by the sample thickness.

We define the overall volume fraction crystallized behind the moving front by

$$f^0(\tau)=\frac{1}{\lambda}\int_0^{\lambda}f(\xi,\tau)d\tau \qquad (6)$$

or for a finite sample

$$f^0(\tau)=\frac{1}{\lambda_p}\int_0^{\lambda_p}f(\xi,\tau)d\tau=\frac{1}{\lambda_p}\int_0^{\lambda}f(\xi,\tau)d\tau+f_1\left(1-\frac{\lambda}{\lambda_p}\right) \qquad (6)$$

LIMITING SOLUTIONS

Short and long time behaviour

Analytical solutions to equations (3a)–(3e) and (4) do not exist. We can derive useful limiting forms, however, for comparison with selected systems. In particular, at 'short' and 'long' times analytical solutions are possible when the crystallization rate, is 'large' or 'small'. For the moment we defer the definition of short and long times or large and small Ω, but develop these limiting solutions for both semi-infinite and finite media.

Initially, swelling kinetics control the transport since molecular diffusion through the thin, penetrated surface layers does not inhibit the swelling process at the moving boundary[2,37,38]. Under these circumstances diffusional gradients behind the moving boundary are negligible and equations (3a)–(3e) reduce to

$$\gamma(0,0)=1$$
$$\gamma(\xi,0)=0 \text{ for } 0<\xi<\lambda$$
$$\gamma(\lambda_s(\tau),\tau)=1;\ \lambda_s(0)=0$$
$$\frac{d\lambda}{d\tau}=\gamma^n;\ \lambda(0)=0 \qquad (7a)$$

These equations govern transport at short times.

At long times diffusion is the governing factor because of the long path to the moving interface for penetrant molecules. In this case significant gradients exist behind the front, and the driving force for swelling is minimal (i.e.

$\gamma(\lambda,\tau)=0$). Under these circumstances the nonlinear moving boundary condition becomes a linear Stefan condition, eliminating the effect of swelling kinetics.

The treatment[37,38] of the analogous problem without crystallization determined the long time behaviour by solving the linear Stefan problem with instantaneous surface saturation as the initial condition. The authors' argument that the long time behaviour of the nonlinear and the corresponding Stefan problems were identical was verified by numerical integration of the former. Similarly we presume that the analogous Stefan problem governs the long time behaviour with crystallization:

$$\begin{gathered}\frac{\partial}{\partial\xi}(1-f)\frac{\partial\gamma}{\partial\xi}=\frac{\partial(1-f)(\gamma+q)}{\partial\tau}\\ \gamma(0,0)=1\\ \gamma(\xi,0)=0 \text{ for } 0<\xi<\lambda\\ \gamma(\lambda_s(\tau),\tau)=1;\ \lambda_s(0)=0\\ -\left.\frac{\partial\gamma}{\partial\xi}\right|_\lambda=q\frac{d\lambda}{d\tau}\end{gathered}\tag{7b}$$

We will subsequently verify this presumption with numerical solutions to equations (3a)–(3e) for large values of Ω which approach the solution to equation (7b).

We will now develop the asymptotic solutions for large and small Ω.

Asymptotic solutions for large Ω

For sufficiently large Ω, the kinetic equation for crystallinity reduces to a jump condition across the moving interface,

$$f(\xi)=f_1+(f_0-f_1)H(\lambda-\xi)\tag{8}$$

where H is the step function. This approximation linearizes the diffusion equation.

The short time asymptote of equations (3a)–(3e) for large values of Ω results from integrating the simplified limit (see equation (7a)) with the jump condition of f:

$$\begin{gathered}\lambda=1\\ \lambda=\lambda_s=\tau\\ \omega=(1-f_0-\varepsilon_0)(1+q)\tau\end{gathered}\tag{9a}$$

The linear dependence of λ and ω on time reflects the initial swelling controlled transport. We can apply these relationships to 'thin' films if the time for film penetration, τ_p, is sufficiently short. Equation (9a) would only apply before complete penetration (i.e. $\lambda<\lambda_p$) and, since no concentration gradients remain when $\lambda=\lambda_p$, sorption is complete at $\tau=\tau_p$.

Combining equations (6), (8) and (9a) gives the overall crystallinity in a thin film, which increases linearly with τ until reaching the ultimate value at τ_p,

$$\begin{gathered}\tau<\tau_p \quad f^0(\tau)=f_1+(f_0-f_1)\left(\frac{\tau}{\tau_p}\right)\\ \tau\geqslant\tau_p \quad f^0=f_0\end{gathered}\tag{9b}$$

Equation (4) then implies that macrovoids result throughout the sample since saturation occurs immediately behind the moving front, hence

$$\varepsilon(\xi)=\varepsilon_0=\frac{v_1^0}{(1-v_1^0)}(f_0-f_1) \text{ for } 0\leqslant\xi\leqslant\lambda_p\tag{9c}$$

Note the void fraction has the maximum possible value.

The asymptotic solutions at long times result from integrating the simplified limit (7b), linearized by the jump condition on f. Solvent conservation at the moving interface gives the appropriate Stefan condition:

$$-\left.\frac{\partial\gamma}{\partial\xi}\right|_\gamma=q\frac{(1-f_1)}{(1-f_0)}\frac{d\lambda}{d\tau}$$

Defining the effective threshold $c^{*\prime}=c^*(1-f_1)/(1-f_0)$ and rescaling the concentration variable $\gamma=(c-c^{*\prime})/(c_0-c^{*\prime})$, allows a convenient representation of the linearized long time limit:

$$\begin{gathered}\frac{\partial^2\gamma}{\partial\xi^2}=\frac{\partial\gamma}{\partial\tau}\\ \gamma(0,0)=1\\ \gamma(\xi,0)=0 \text{ for } 0<\xi<\lambda_p\\ \gamma(0,\tau)=1\\ -\left.\frac{\partial\gamma}{\partial\xi}\right|_\lambda=Q\frac{d\lambda}{d\tau}\end{gathered}\tag{10}$$

Q and q are related by

$$\frac{1}{Q}\simeq\frac{(1-f_0)}{q}-f_0$$

when f_1 is small compared to f_0. In addition to the criteria developed for long times and large Ω, we require

$$\frac{q}{(1+q)}<(1-f_0)$$

for equations (8) and (10) to replace equation (3).

The methods discussed by Dankwerts[44] yield the following dimensionless solutions to equation (10) for the concentration profiles, penetration distance and weight gain in semi-infinite media:

$$\begin{gathered}\gamma=1-\frac{erf\,\xi/2\sqrt{\tau}}{erf\,M}\\ \lambda=2M\sqrt{\tau}\\ \omega=2M(1-f_0)Q\,e^{M^2}\sqrt{\tau}\end{gathered}\tag{11a}$$

M is given implicitly by

$$\frac{1}{Q}=(\pi)^{1/2}M\,e^{M^2}\,erf\,M$$

The $\sqrt{\tau}$ dependence in equation (11a) reflects the diffusional impedances inherent in the long time behaviour.

Equations (11a) readily adapt to the case of films thick enough that the time for complete penetration of the

specimen satisfies the criteria for long times. Since we ignore solvent in the unpenetrated portion of the film, equations (11a) apply directly for $\tau<\tau_p$ (i.e. $\lambda<\lambda_p$). When $\tau>\tau_p$, the penetration kinetics obviously terminate, as do the crystallization kinetics represented through the jump condition on f. However, equations (11a) evaluated at τ_p reveal concentration gradients which drive further sorption after penetration. We resolve the continued dynamics by solving equation (10) as an initial-boundary value problem with a no flux condition at the centreline and the solution coinciding with the concentration profiles in equations (11a) at τ_p. The results describe the decay of the concentration gradients and the additional weight gain after the complete penetration of the film as

$$\gamma=1-\frac{2}{\mathrm{erf}M}\sum_{n=0}^{\infty}A_n e^{-(k_n/\lambda_p)^2(\tau-\tau_p)}\sin k_n\frac{\xi}{\Lambda_p}$$

$$\frac{\omega(\tau>\tau_p)}{\omega(\infty)}=1-\frac{2}{\mathrm{erf}M(1+Q)}\sum_{n=0}^{\infty}A_n e^{-(k_n/\lambda_p)^2(\tau-\tau_p)} \tag{11b}$$

where

$$\tau_p=\lambda_p^2/4M^2$$

$$k_n=\frac{(2n+1)}{2}\pi \qquad n=0,1,2\ldots$$

$$A_n=\frac{1}{k_n}e^{-(k_n/2M)^2}-\frac{1}{k_n}e^{M^2}(-1)^n R_e\left(iw\left(\frac{k_n}{2M}+iM\right)\right)$$

with R_e representing the real part of the argument containing the complex error function w[45]. (If we recall that γ is scaled on the effective threshold concentration, $c^{*\prime}$, in equation (11b)).

The corresponding predictions of the overall crystallinity result from combining equations (6), (8) and (11a) into

$$\tau<\tau_p \quad f^0(\tau)=f_1+(f_0-f_1)\left(\frac{\tau}{\tau_p}\right)^{1/2}$$

$$\tau\geqslant\tau_p \quad f^0=f_0 \tag{11c}$$

So, we find diffusionally limited crystallization kinetics.

Finally we apply equation (4) to predict the final morphology. The jump condition on f and the concentration profiles predicted in equation (11a) indicate that crystallization is complete before local saturation, except at the surface which is saturated initially. Hence, cavitation with the maximum possible value is predicted only at the surface

$$\varepsilon(\xi)=\varepsilon_0=\frac{v_1^0}{(1-v_1^0)}(f_0-f_1) \qquad \text{for } \xi=0$$

$$\varepsilon=0 \qquad \text{for } 0<\xi<\lambda_p \tag{11d}$$

Behaviour for small Ω

For small Ω in finite media crystallization occurs on a much longer time scale than does transport, so the processes decouple. Hence, crystallization does not influence the transport process and therefore equations (3) reduce to Astarita and Sarti's description of anomalous diffusion in non-crystallizable, glassy polymers[37]. Their short and long time asymptotes resemble those just presented; swelling kinetics control at short times while molecular diffusion controls at long times. Adaptations to finite media (thick and thin films) are obvious.

For small values of Ω, crystallization occurs subsequent to saturation in any finite sample, so the specimen crystallizes as a saturated bulk. The lumped parameter version of the crystallization equation in equations (3), with $h(\gamma)$ evaluated at $\gamma=1$, describes the variation of f with time. Integration gives

$$\Omega\tau f_0^{2/3}h(1)=\frac{1}{3}\ln\frac{\left[1+\left(\frac{f}{f_0}\right)^{1/3}+\left(\frac{f}{f_0}\right)^{2/3}\right]^{1/2}}{1-\left(\frac{f}{f_0}\right)^{1/3}}$$

$$-\frac{\sqrt{3}}{3}\left[\frac{\pi}{6}-\tan^{-1}\frac{2\left(\frac{f}{f_0}\right)^{1/3}+1}{\sqrt{3}}\right] \tag{12}$$

when f_1 is nearly zero. Equation (12) closely matches the corresponding Avrami expression[46,47]; displaying the characteristic sigmoidal kinetic curve usually associated with bulk crystallization. *Figure 2* shows the comparison for methylene chloride in PET at 22°C and a volume fraction of 0.4.

Uniform cavitation at the maximum value throughout the sample should result according to (4) since $f^c=f_1$.

Criterion for application of asymptotic solutions in finite media

We now define four distinct sets of criteria for the validity of the four limiting cases in finite media: thin and thick films for large values of Ω, and thin and thick films for small values of Ω.

Large Ω. The time when the asymptotic limits for the weight gain in thin and thick films coincide, τ_c, serves as an estimate for the change over from linear to square root of time dependence in the weight gain[37]. In the case of fast

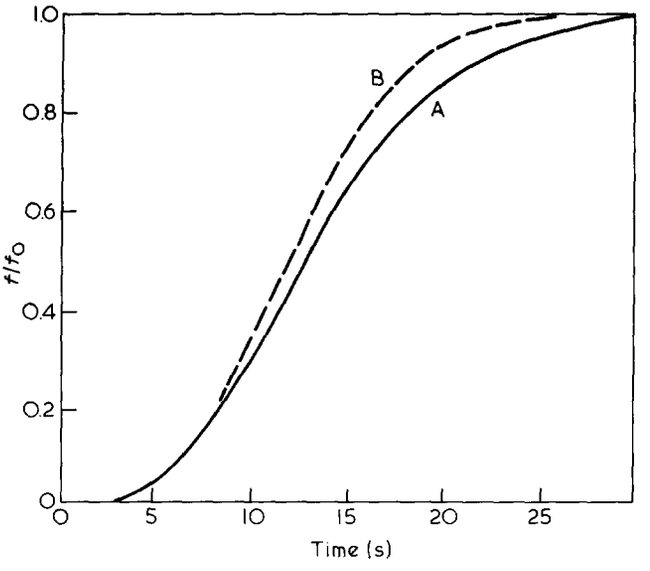

Figure 2 Comparison of equation (12) (curve A) with the corresponding Avrami expression (curve B) for methylene chloride in PET at 22°C and a volume fraction of 0.40

crystallization, combining the weight gain in equation (9a) with that in equation (11a) gives

$$\tau_c = 4M^2 e^{2M^2} \left\{ \frac{(1-v_1^0)(1-f_0)}{(1-v_1^0-f_0)} \frac{Q}{1+q} \right\}^2 \quad (13)$$

where equation (4) with $f^c = 0$ has been used for ε_0. Substitution into the equations for penetration depth in equations (9a) and (11a) then yield the desired thickness criteria for thin film behaviour as

$$\lambda_p \ll 4M^2 e^{2M^2} \left\{ \frac{(1-v_1^0)(1-f_0)}{(1-v_1^0-f_0)} \frac{Q}{(1+q)} \right\}^2 \quad (14a)$$

and for thick film behaviour as

$$\lambda_p \gg 4M^2 e^{M^2} \frac{(1-v_1^0)(1-f_0)}{(1-v_1^0-f_0)} \left\{ \frac{Q}{(1+q)} \right\} \quad (14b)$$

Strict inequalities (i.e. $\ll$ or $\gg$) are appropriate since, as shown subsequently, the transition from thin to thick behaviour is actually quite gradual.

Of course these criteria apply only for sufficiently large Ω to justify the jump condition on f. To judge this, the kinetic equation for f in equation (3) must be rescaled using the characteristic time for film penetration. If the resulting renormalized crystallization rate is sufficiently large use of the jump condition is permissible.

For thin films, rescaling the governing transport equations in (7a) with

$$\bar{\xi} = \xi/\lambda_p = x/\Lambda_p$$

$$\bar{\tau} = \tau/\lambda_p = tU_0/\Lambda_p$$

gives $\lambda_p\Omega$ for the renormalized crystallization rate. Therefore

$$\lambda_p\Omega \gg 1 \quad (15a)$$

justifies the jump condition. Hence conditions (14a) and (15a) are both necessary for the thin film, large Ω asymptotes (9) to be applicable. Since

$$\lambda_p\Omega = \frac{\Lambda_p}{U_0} \frac{36\pi N_s^{1/3} G_0 S}{V_E \quad f_0}$$

$$= \frac{\text{time scale for swelling controlled transport}}{\text{time scale for crystallization}}$$

condition (15a) implies swelling controlled crystallization, which requires extremely large values of Ω.

For thick films, rescaling the transport equations in (7b) with

$$\bar{\xi} = \xi/\lambda_p = x/\Lambda_p$$

$$\bar{\tau} = \tau/\lambda_p^2 = tD/\Lambda_p^2$$

gives $\lambda_p^2\Omega$ for the renormalized crystallization rate. So,

$$\lambda_p^2\Omega \gg 1 \quad (15b)$$

assures that the jump condition properly represents crystallization. Since

$$\lambda_p^2\Omega = \frac{\Lambda_p^2}{D} \frac{36\pi N_s^{1/3}}{V_E} \frac{G_0 S}{f_0}$$

$$= \frac{\text{time scale for diffusion controlled transport}}{\text{time scale for crystallization}}$$

condition (15b) corresponds to diffusion controlled crystallization kinetics, exactly consistent with the mathematical limits derived earlier (see equation (11)). Furthermore, $\lambda_p^2\Omega$ depends on the square of the film thickness, implying thicker films will tend to display rapid crystallization behaviour and diffusionally limited crystallization kinetics. The combination $\lambda_p^2\Omega$ is exactly analogous to the parameter in Zachmann's model[7] which determines the relative influence of diffusion on the crystallization kinetics. Hence, Zachmann's analysis implicitly assumes the condition shown by condition (14b).

Small values of Ω. We will now obtain the criteria for thick and thin films in the case of small values of Ω following the procedure used above. Because transport largely precedes crystallization in this case, the criteria follow directly from the results of Astarita and Sarti[37]. Specifically, for thin films

$$\lambda_p \ll 4m^2 e^{2m^2} \left(\frac{q}{1+q} \right)^2, \quad (16a)$$

while for thick films the following condition

$$\lambda_p \gg 4m^2 e^{m^2} \frac{q}{(1+q)} \quad (16b)$$

must be satisfied, where m is defined by

$$\frac{1}{q} = (\pi)^{1/2} m e^{m^2} \text{erf} m$$

In addition, the conditions for small values of Ω follow from the rescaling procedure. With condition (16a) for thin films:

$$\lambda_p\Omega \ll 1 \quad (17a)$$

is needed and with condition (16b) for thick films

$$\lambda_p^2\Omega \ll 1 \quad (17b)$$

is needed.

Note that slow crystallization in thick films requires extremely small values of Ω since conditions (16b) and (17b) must be simultaneously satisfied. Also, since the lefthand side of equation (17a) depends directly on the film thickness, thin films will tend to display overall crystallization controlled by the spherulite growth rate.

Table 3 summarizes the results.

Numerical calculations for large values of Ω

Equations (3a)–(3e) have been solved numerically for the penetration depth and concentration distributions using finite difference methods, discussed elsewhere[29]. A trapezoidal rule approximation of equation (5) gives the weight gain kinetics. We now compare briefly the

Table 3 Asymptotic formulas for diffusion with induced crystallization in films

Case	Description	Criteria	Weight gain	Crystallization	Macrovoids
A	thick films, fast crystallization	(14b), (15b)	diffusion controlled	diffusion controlled	surface only
B	thin films, slow crystallization	(16a), (17a)	swelling controlled	spherulite growth controlled	uniform throughout specimen
C	thin films, fast crystallization	(14a), (15a)	swelling controlled	swelling controlled	uniform throughout specimen
D	thick films, slow crystallization	(16b), (17b)	diffusion controlled	spherulite growth controlled	uniform throughout specimen

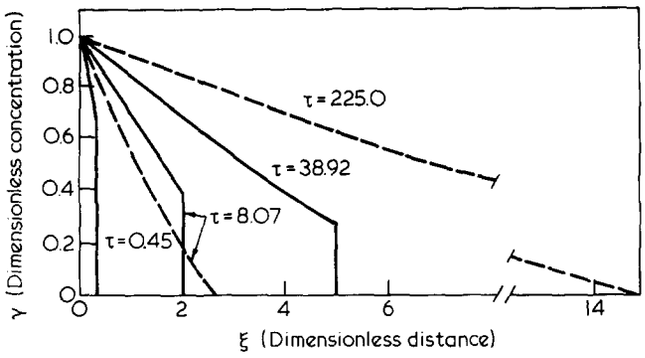

Figure 3 Evolution of concentration profiles with time. (——) numerical solution of (3); (-----) thick film asymptotic solution for large Ω(case A). Model parameters are given in the text

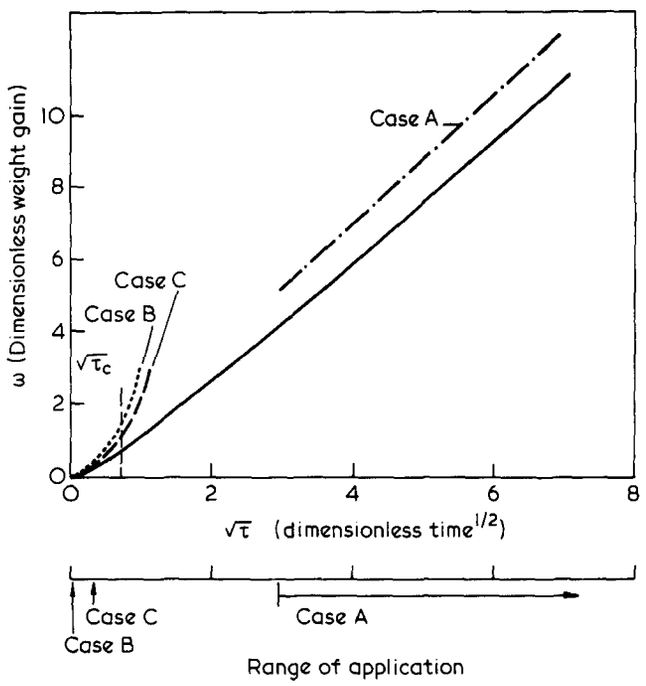

Figure 4 Dimensionless weight gain, ω, *versus* the square root of the dimensionless time, $\sqrt{\tau}$. (——) numerical solution of (3); (— — —) thin film asymptotic solution for large Ω (case C); (- - - - -) thin film asymptotic solution for small Ω (case B); (—·—·—) thick film asymptotic solution for large Ω (case A). τ_c from (13) is also shown. Model parameters are given in the text

behaviour of equation (3) with the asymptotic solutions using reasonable model parameters[34]: $\Omega=80$, $q=1.5$, $n=2.0$, $f_0=0.10$, $f_1=0.05$ and $h(\gamma)$ evaluated for methylene chloride in PET having a volume fraction of 0.4 in the amorphous component at saturation.

The numerical calculations are for a semi-infinite slab, but apply to finite films for times less than the penetration time, τ_p, since the model neglects solvent transport ahead of the moving boundary. Therefore, one can compare the numerical and asymptotic predictions for $0<\tau<\tau_p$, where the limiting conditions, (14–17), and the corresponding asymptotic expressions for $\lambda_p(\tau_p)$ define τ_p. Considering $\ll$ and $\gg$ to be satisfied by an order of magnitude difference, for the parameters specified, case A applies if $\tau_p>8$, case B if $\tau_p<0.001$, and case C if $\tau_p\cong 0.1$; the conditions for case D cannot be satisfied. When appropriate, subsequent plots show the bounds on τ_p along the time axis.

Figure 3 shows the concentration profiles evolving with time, giving a clear picture of the transition from swelling controlled behaviour to diffusion control. The profiles to the left show a large discontinuity corresponding to the substantial driving force for the swelling process at the glass/rubber interface. The swelling kinetics dictate the dynamics of sorption since the path for migration of solvent to the boundary is minimal. As the penetration depth increases, molecular diffusion from the surface begins to limit the supply of diluent to the boundary, curbing the driving force for swelling. The velocity of the front diminishes, and the profiles behind the interface begin to display typical parabolic shapes. At very long times the extended path for molecular migration through the penetrated rubber causes solvent diffusion to control the transport. The dashed lines in *Figure 3* show profiles calculated from the thick film, fast crystallization asymptote, illustrating the approximation for $\tau\cong 8$ and the gradual decay of the discontinuity at the moving interface.

Figure 4 shows the weight gain plotted against the square root of time, the common representation of experimental data. The numerical and analytical results agree closely for small τ_p (cases B and C) and fairly well for large τ_p (case A). The latter agreement improves as τ_p is made larger, supporting the earlier presumption that the Stefan problem (equation (7b)) adequately represents the model for long times. The critical time calculated from equation (13), τ_c, appears to be a valid estimate for the change over from swelling to diffusion control.

Figure 5 shows the sample half depth, λ_p, versus the time for penetration of the film, τ_p. For the limit of rapid crystallization in thin films (case C), the criteria are quite restrictive, limiting the asymptotic representation to $\tau_p\cong 0.1$, where the numerical and asymptotic results show gratifying agreement. Rapid crystallization in thick films requires the condition $\tau>8$ to be filfilled; so that the equations in (11) fit for an infinite range of λ_p.

Similarly, for slow crystallization, the criteria for thick

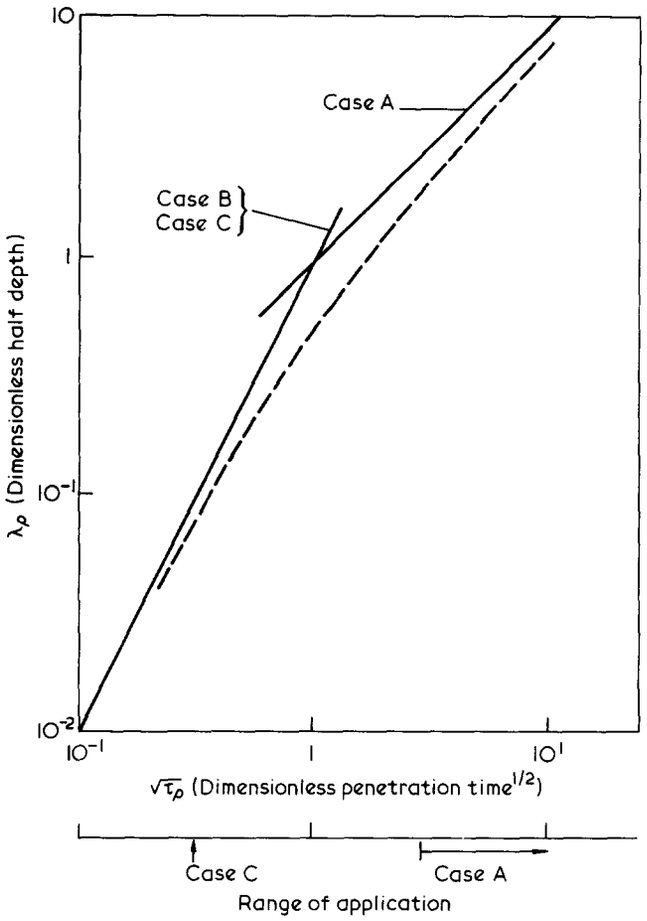

Figure 5 Dimensionless sample half depth, λ_p, *versus* the dimensionless penetration time, τ_p. (-----) numerical solution to (3); (——) asymptotic solutions (cases A, B and C). Model parameters are given in the text.

films (case D) are more restrictive than for thin films (case B). Clearly the criteria for cases C and D limit their practical utility.

Figure 5 also shows the transition between the asymptotic limits to be quite gradual, and illustrates that a considerable domain outside the range of the analytical approximations exists. Determining the model's behaviour therein motivates a parameteric study of equation (3) via numerical simulation. This is discussed in another article[29].

CONCLUSIONS

The model presented herein accommodates the features observed during diffusion with induced crystallization. Specifically, the description is consistent with

(a) existence of a threshold activity[2],
(b) appearance of moving boundaries[8,9,16,17,22]
(c) penetration depth and weight gain increasing linearly with $\sqrt{t}$ in thick films[8,9,17,19,20],
(d) continued weight gain after complete penetration in thick films[9],
(e) initial weight gain increasing linearly with time in thin films[14,15,19,22],
(f) surface macrovoids produced by liquid contact[8,9,20],
(g) internal macrovoids in thin films[12,19].

The physics underlying the model allow clear interpretations of several experimental observations. We have identified the threshold activity for crystallization with that needed to initiate propagation of the moving boundary. The cracking near the moving boundary in PET[9] and PC[16,17] systems corresponds to yielding and/or failure of the glassy polymer under osmotic stresses.

The asymptotic analysis identified four limiting types of behaviour for the process in finite media (*Table 3*). Cases A and B probably account for most practically encountered systems owing to the very restrictive criteria for cases C and D.

The combination of features predicted by case A is readily observed in several PET systems[8,9]. These simultaneously show penetration depth, weight gain and overall crystallinity increasing linearly with $\sqrt{t}$, and macrovoids restricted to surface layers only. Here, the model suggests that a long diffusion path develops between the film's surface and the moving boundary, producing diffusion controlled transport and crystallization. The solvent occluded from crystallites during rapid crystallization just behind the front is accommodated by partially swollen polymer, inhibiting the formation of internal macrovoids.

Similarly, thin PC films[14,15,19] show the features predicted by case B. Here, case II weight gain occurs initially and macrovoids develop internally. The model suggests the swelling process controls the transport since no gradients develop behind the front. Internal macrovoids result since the polymer crystallizes from a fully swollen state.

Numerical calculations demonstrate that a considerable region between the limiting cases exists, requiring numerical simulations to determine the model's behaviour. These, and comparisons of the model's predictions with published experimental results, are presented elsewhere[29].

NOMENCLATURE

B = blocking factor.
c = local mass concentration of diluent in amorphous polymer.
c_0 = ultimate solubility of diluent in amorphous polymer.
c^* = threshold concentration, glassy side.
c^* = threshold concentration, rubbery side.
$c^{*\prime}$ = effective threshold, rubbery side.
D_E = effective diffusion coefficient of diluent, polymer fixed frame.
D = effective amorphous domain diffusion coefficient, polymer fixed frame.
D_a = amorphous domain diffusion coefficient, polymer fixed frame.
f = local volume fraction crystallized.
f_0 = ultimate crystallinity.
f_1 = volume fraction nuclei.
f^c = crystallinity when saturation first occurs.
G = radial growth rate of a spherulite.
G_{max} = maximum value of G for $c^* < c < c_0$.
G_0 = preexponential constant in expression for G.
K = empirical constant in rate expression for Λ.
l = characteristic length of local amorphous domains.
n = empirical exponent in rate expression for Λ.
N_s = number of spherulites in a volume element.

r = radius of spherulite.
S = G_{max}/G_0.
t = lab time.
t^* = characteristic time scale for transport.
t_p = penetration time = time for moving boundary to reach the film's centreline.
u = mass average velocity.
v_1^0 = ultimate volume fraction diluent in amorphous domains.
V_E = volume of a crystallizing volume element.
V_S = volume of a single spherulite.
V_T = total volume of spherulites in a volume element.
V_T^0 = maximum total volume available to spherulites in a volume element.
W = weight gain per unit cross section.
x = distance into polymer from surface.
x^* = characteristic length scale for transport.
x^0 = final overall mass fraction sorbed by polymer.

GREEK SYMBOLS

ε = local void fraction.
Ψ = geometric impedance factor.
Λ = position of moving boundary.
Λ_p = half thickness of film.
ρ = polymer mass density.
ρ^* = polymer mass density at the threshold concentration.
ρ_0 = ultimate polymer mass density.
$\Delta\rho = \rho - \rho^*$ = local change in polymer mass density from the value at the threshold.
$\Delta\rho_0$ = ultimate change in polymer mass density.
ρ_a = dry, amorphous polymer density.
ρ_c = pure crystalline polymer density.
ρ_s = pure solvent density.

DIMENSIONLESS VARIABLES AND PARAMETERS

Γ = change in polymer density.
γ = diluent concentration in amorphous polymer.
ξ = distance.
$\bar{\xi}$ = rescaled distance in films.
λ = position of the moving boundary.
λ_s = position of the saturation boundary line.
λ_p = sample half depth.
ρ_s^* = solvent density.
τ = time.
$\bar{\tau}$ = rescaled time in films.
τ_p = penetration time.
v = mass average velocity.
q = threshold concentration.
Q = effective threshold concentration.
Ω = crystallization rate.
ω_T = total weight gain.
ω_a = weight gain in amorphous polymer.

ACKNOWLEDGEMENTS

The authors thank Professor L. Rebenfeld and Dr H. D. Weigmann of the Textile Research Institute for their valuable input. We gratefully acknowledge the National Science Foundation for financial support (Grant No. DMR-7905980).

REFERENCES

1 Knox, B. H., Weigmann, H.-D. and Scott, M. G. *Text. Res. J.* 1975, **45**, 203
2 Durning, C. J., Scott, M. G. and Weigmann, H.-D. *J. Appl. Polym. Sci.* 1982, **27**, 3597
3 Frisch, H. L. *Polym. Eng. Sci.* 1980, **20**, 2
4 Baker, W., Fuller, G. and Pape, N. *J. Am. Chem. Soc.* 1942, **61**, 766
5 Moore, W. R. and Sheldon, R. P. *Polymer* 1961, **2**, 315
6 Sheldon, R. P. *Polymer* 1962, **3**, 27
7 Zachmann, H. G. and Konrad, G. *Makromol. Chemie.* 1968, **118**, 189
8 Desai, A. B. and Wilkes, G. L. *J. Polym. Sci. Symp.* 1974, **46**, 291
9 Makarewicz, P. J. and Wilkes, G. L. *J. Polym. Sci., Polym. Phys. Edn.* 1978, **16**, 1529
10 Makarewicz, P. J. and Wilkes, G. L. *J. Polym. Sci., Polym. Phys. Edn.* 1978, **16**, 1559
11 Jameel, H., Waldman, J. and Rebenfeld, L. *J. Appl. Polym. Sci.* 1981, **26**, 1975
12 Jameel, H., Noether, H. and Rebenfeld, L. *J. Appl. Polym. Sci.* 1982, **27**, 773
13 Mercier, J. P., Groeninckx, G. and Lesne, M. *J. Polym. Sci. C* 1967, **16**, 2059
14 Kambour, R. P., Karasz, F. E. and Daane, J. H. *J. Polym. Sci. A-2* 1966, **4**, 327
15 Titow, W. V., Braden, M., Currel, B. R. and Loneragan, R. J. *J. Appl. Polym. Sci.* 1974, **18**, 867
16 Turska, E. and Benecki, W. *J. Polym. Sci. Symp.* 1974, **44**, 59
17 Turska, E. and Benecki, W. *J. Appl. Polym. Sci.* 1979, **23**, 3489
18 Turska, E. and Janeczek, J. *Polymer* 1979, **20**, 355
19 Ware, R., Tirtowidjojo, S. and Cohen, C. *J. Appl. Polym. Sci.* 1981, **26**, 2975
20 Wilkes, G. L. and Parlapiano, J. *Polym. Prepr.* 1976, **17**, 937
21 Makarewicz, P. J. and Wilkes, G. L. *J. Appl. Polym. Sci.* 1978, **22**, 3347
22 Overbergh, N., Berghmans, H. and Smets, G. *Polymer* 1975, **16**, 703
23 Turska, E. and Janeczek, H. *Polymer* 1978, **19**, 816
24 MacNulty, B. J. *J. Polym. Sci. A-1* 1969, **7**, 3038
25 Alfrey, T., Gurnee, E. F. and Lloyd, W. G. *J. Polym. Sci. C* 1966, **12**, 249
26 Sarti, G. C. *Polymer* 1979, **20**, 827
27 Thomas, N. L. and Windle, A. H. *Polymer* 1980, **21**, 613
28 Thomas, N. L. and Windle, A. H. *Polymer* 1982, **23**, 529
29 Durning, C. J. and Russell, W. B. *Polymer* 1985, **26**, 131
30 Hoffman, J. D. and Lauritzen, J. I. *J. Res. Natl. Bur. Std. A* 1961, **65A**, 297
31 Lawton, E. L. and Cates, D. M. *Text. Res. J.* 1978, **48**, 478
32 Ryan, E. G. and Calvert, P. D. *Polymer* 1982, **23**, 877
33 Peterlin, A. *J. Macromol. Sci. Phys.* 1975, **B11**(1), 57
34 Durning, C. J., Ph.D. Thesis, 1983, Department of Chemical Engineering, Princeton University, Princeton, New Jersey
35 Sarti, G. C. and Apicella, A. *Polymer* 1980, **21**, 1031
36 Crank, J. in 'The Mathematics of Diffusion', 1956, Clarendon Press, Oxford, p. 223
37 Astarita, G. and Sarti, G. C. *Polym. Eng. Sci.* 1978, **18**, 388
38 Astarita, G. and Joshi, S. *J. Memb. Sci.* 1978, **4**, 165
39 Micheals, A. S., Vieth, W. and Barrie, J. A. *J. Appl. Phys.* 1963, **34**, 13
40 Klute, C. H. *J. Polym. Sci.* 1959, **41**, 307
41 Lasoski, S. L. and Cobbs, W. H. *J. Polym. Sci.* 1959, **36**, 21
42 Fujita, H. *Fortsch. Hoch. Polym. Forsch.* 1964, **3**, 1
43 Stein, R. S. and Mirsa, A. *J. Polym. Sci., Polym. Phys. Edn.* 1973, **44**, 409
44 Dankwerts, P. V. *Trans. Faraday Soc.* 1950, **46**, 701
45 Abramowitz, M. and Stegun, I. A. 'Handbook of Mathematical Functions', Dover Publ., New York, 1964, Ch. 7
46 Mandelkern, L. in 'Crystallization of Polymers', McGraw-Hill, New York, 1964, Ch. 8
47 Turnbull, D. in 'Solid State Physics', V.3, (Eds. F. Seitz and D. Turnbull), Academic Press Inc., New York, 1956, p. 225